

Polarization Mode Dispersion in High-Speed Optical Communication Systems

M. F. FERREIRA
A. N. PINTO
P. S. ANDRÉ
N. J. MUGA

University of Aveiro
Aveiro, Portugal

J. E. MACHADO

PT Inovação, S.A.
Aveiro, Portugal

R. N. NOGUEIRA
S. V. LATAS
M. H. SOUSA
J. F. ROCHA

University of Aveiro
Aveiro, Portugal

We review the research progress concerning some fundamental issues related to polarization-mode dispersion (PMD) in high-speed fiber-optic transmission systems. We pay particular attention to issues such as the PMD-induced pulse broadening, PMD measurement and emulation, as well as PMD compensation. An electrical equalization technique based on a transversal filter and an optical technique based on a nonlinear chirped fiber Bragg gratings for PMD compensation will be discussed.

Keywords optical fiber communications, polarization-mode dispersion, PMD statistics, PMD measurements, PMD emulation, PMD equalization, PMD compensation

Introduction

The phenomenon of polarization-mode dispersion (PMD) is now considered to be one of the main limiting factors for high-speed long-haul lightwave transmission systems, especially for systems with bit rate of 40 Gb/s per channel and beyond [1–3]. The origin

Received 25 November 2004; accepted 25 November 2004.

Address correspondence to M. F. Ferreira, Physics Department, University of Aveiro, Campus de Santiago, Aveiro 3810-193, Portugal. E-mail: mferreira@fis.ua.pt

of PMD is the small random birefringence in the optical fiber caused by imperfections in the manufacturing process and/or mechanical stress on the fiber after manufacture. This birefringence leads to different dispersion relations for the two orthogonal polarized modes of the fiber [4]. Besides that, the random change of birefringence along the fiber results in random coupling between the modes.

Typically, PMD is represented by a vector that has a magnitude equal to the differential group delay (DGD), $\Delta\tau$, which is the time delay between the two orthogonal principal states of polarization (PSP) [5]. Neglecting variations in the PMD vector with respect to frequency, first-order PMD is obtained. However, in real fibers, both the magnitude and direction of the PMD vector change with frequency, meaning that higher-order PMD must generally be considered.

There is a large interest in techniques to compensate for or mitigate the effects of PMD, and a number of methods have been proposed. The main problem is the temporal random change of the PMD, which forces any compensation technique to dynamically adapt while the system is running.

Transmission fibers have random birefringence; i.e., a birefringence whose main axes and strength change along the fiber and time in a random manner. In long fibers, the statistical probability distribution of the DGD is Maxwellian [6] and the average DGD grows as the square root of the fiber length [7]. Since its nature is essentially random, the most common way to treat PMD mathematically is by mean of statistics [6, 8, 9].

In this article we review recent research related to PMD. The basic theory of PMD is presented. Moreover, the impairments from PMD, as well as the compensation methods, are discussed in terms of root-mean-square (rms) pulse broadening. We address the problem of PMD measurement. Due to the statistical nature of PMD, it is difficult to assess the performance of a PMD compensator in a real fiber communication system. A PMD emulator makes possible such assessment. A review of the main PMD emulator types is presented and describes a novel configuration. The final part of the article is dedicated to the PMD compensation issue. First, an electrical transversal filter is used, and afterwards a dynamical optical compensation technique using nonlinear chirped fiber Bragg gratings is presented. Finally, the main conclusions of the article are summarized.

Theory

PMD Fundamentals

PMD is caused by optical birefringence and its variation along optical fibers. The birefringence in single-mode optical fibers destroys the degeneracy of the two orthogonal polarized modes, leading to different propagation delays. Due to the fact that pulses couple with both modes, difference in the delays leads to pulse broadening. When the difference in the delays approaches a significant fraction of the bit period, strong system penalties occur.

An ideal single-mode fiber supports two degenerated orthogonal polarized modes. Due to the degenerated characteristic of these modes, coherent light maintains its state of polarization (SOP). However, the perfect circular shape that is required for the degeneracy of the orthogonal modes is not achieved in practice. Some asymmetry in the fiber always exists leading to a difference in the propagation constant of the two orthogonal modes.

A more realistic model for the fiber is obtained considering that the fiber core has an elliptical shape instead of circular one. In the elliptical shape model is possible to

define two main axes, coincident with the physical axes, having different propagation constants. If coherent linearly polarized light is launched in a direction not coincident with one of this principal axes, light couples with both modes. In this situation, light polarization goes from linear to various states of elliptical polarization before returning again to its original linear polarization. The light goes through this cycle periodically because the phase difference $\phi_y - \phi_x$ varies periodically due to the fact that $\beta_y - \beta_x$ is not zero but is constant, ϕ_x, β_x and ϕ_y, β_y represent, respectively, phase of the electrical field and propagation constant in the x and y axis. The transmission length associated with this oscillation in the light polarization is known as the beat length (L_b). Standard telecommunications fibers, for wavelengths (λ) around 1550 nm, have for the orthogonal modes a relative refraction index difference ($\Delta n/n$) of the order of $\sim 10^{-7}$ leading to beat lengths ($L_b = \lambda/\Delta n$) of the order of ~ 10 m [10]. The quantity $\Delta n = |n_x - n_y|$, sometimes represented by a capital B , is known as the fiber birefringence. In the latest definition it was assumed that the x and y direction were made coincident with the slow and fast axis of the elliptical core fiber.

However, in practice, this periodical behavior is not observed in a fiber with small birefringence. This is due to the fact that the perturbation that induces the birefringence does not remain constant. Indeed, this perturbation is a random process, with roots in the lack of control at the fabrication and deployment of the fiber and cables.

Therefore, a more suitable model to describe the evolution of polarization is a concatenation model in which small pieces of elliptical fibers with uniform birefringence are randomly rotated and concatenated. With this concatenation model, light polarization through propagation in an optical fiber does not present a periodical behavior.

In the concatenation model, the random nature of the polarization evolution appears only along the propagation distance. Therefore, the different polarization states of light can in principle be deduced from the complete knowledge of the birefringence along the fiber. However, neither is it frequently possible to obtain this knowledge in practice nor does the birefringence remain invariant with time. Indeed, birefringence is very sensitive to external conditions as mechanical stress and temperature. For that reason, in the model used to describe birefringence in long fibers, a random process is also introduced in the time domain. Therefore, besides the random rotation along the propagation distance the perturbation that produces the birefringence is also a random process, leading to a random rotation of the axes with time.

The concatenation model with random mode-coupling subjected to random perturbations only allows a statistical treatment. A quantity known as the correlation length, L_c , is used to describe how effective this random mode-coupling is in terms of propagation distance. L_c is defined as that length where the power difference has decayed to $\langle p_x \rangle - \langle p_y \rangle = 1/e^2$, assuming $\langle p_x \rangle = 1$ and $\langle p_y \rangle = 0$ at the input, where $\langle p_x \rangle$ and $\langle p_y \rangle$ are averages of the optical power measured in the x and y axes, respectively. Correlation lengths can be less than 1 m when fiber is spooled, due to the large amount of polarization mode coupling, and can be ~ 1 km when fiber is cabled [4].

With this concatenation model with random mode-coupling subjected to random perturbations, it is virtually impossible to predict light polarization in long fibers, as the ones used typically in telecommunications systems. Nevertheless, the final polarization state of the light is not a major concern in current direct detection receivers, as these receivers are insensitive to the state of polarization. What affects such receivers is not the random polarization state of light, but the pulse broadening due to PMD.

The birefringence changes randomly along the fiber length but it is possible to define a special orthogonal pair of polarization at the fiber input called the “principal

states of polarization" (PSPs). Light launched in a PSP does not change depolarization at the output when wavelength is slightly varied. These PSP modes have different group delays, τ_g , which are the maximum and minimum mean time delays in the time domain view. The difference between the two delays is called the differential group delay (DGD) and characterizes the first-order PMD effects.

Using the Principal States Model [4], PSPs and DGDs may both be described by the PMD vector, $\mathbf{\Omega}$. The PMD vector is just a vector in the Stokes space pointing in the direction of the fast PSP, with length equal to the differential group delay, $\Delta\tau$.

The statistical theory of PMD has provided an elegant expression linking the mean square DGD as a function of the propagation distance, L , with L_b and L_c [10]:

$$\langle \Delta\tau^2 \rangle = 2 \left(\Delta\tau_b \frac{L_c}{L_b} \right)^2 \left(\frac{L}{L_c} + e^{-L/L_c} - 1 \right) \quad (1)$$

where $\Delta\tau_b = L_b \Delta n / c$ is the DGD for a single beat length and c is the speed of light in vacuum.

It is interesting to note that when $L \ll L_c$, corresponding to the so-called short-distance regime, the PMD grows linearly with the transmission distance. On the other hand, when $L \gg L_c$ (the long-distance regime), the PMD grows with the square root of L . In the last case, the mean square root of DGD is given by $\Delta\tau_{\text{rms}} = \sqrt{\langle \Delta\tau^2 \rangle} = D_p \sqrt{L}$, where D_p is the PMD coefficient.

Furthermore, in long-distance regime fibers, the probability density function (pdf) of DGD is Maxwellian [6]:

$$p(\Delta\tau) = \frac{8}{\pi^2 \langle \Delta\tau \rangle} \left(\frac{2\Delta\tau}{\langle \Delta\tau \rangle} \right)^2 e^{-\left(\frac{2\Delta\tau}{\langle \Delta\tau \rangle}\right)^2 \frac{1}{\pi}} \quad (2)$$

where $\langle \Delta\tau \rangle$ is the mean DGD. The mean DGD is related to $\Delta\tau_{\text{rms}}$ by the expression $\langle \Delta\tau \rangle = \sqrt{\frac{8}{3\pi}} \Delta\tau_{\text{rms}}$.

PMD-Induced Pulse Broadening

A well-known manifestation of PMD is that optical pulses broaden by an amount that is dependent on the launched SOP. The rms pulse width broadened due to the PMD is given by [11]:

$$\tau^2 = \tau_o^2 + \frac{1}{4} [\langle \mathbf{\Omega}^2 \rangle - (\mathbf{s} \cdot \langle \mathbf{\Omega} \rangle)^2] \quad (3)$$

where τ_o is the initial rms pulse width, \mathbf{s} is the input SOP (Stokes vector), and the bracket denotes frequency average. Equation (3) includes all order PMD effects and does not depend on the pulse shape. We define an expected rms broadening factor b as

$$b^2 = E \left[\frac{\tau^2}{\tau_o^2} \right] = 1 + \frac{1}{4\tau_o^2} [E\{\langle \mathbf{\Omega}^2 \rangle\} - E\{(\mathbf{s} \cdot \langle \mathbf{\Omega} \rangle)^2\}] \quad (4)$$

where $E\{\cdot\}$ denotes expectation value. From Equation (4), the broadening factor due to the PMD is given by [12]:

$$b^2 = 1 + \frac{1}{4\tau_o^2} \left[E\{\Delta\tau^2\} - \frac{1}{3} \int_{-\infty}^{\infty} \int_{-\infty}^{\infty} g(\omega_1 - \omega_2) \frac{|\tilde{f}(\omega_1)|^2 |\tilde{f}(\omega_2)|^2}{4\pi^2} d\omega_1 d\omega_2 \right] \quad (5)$$

where $g(\omega_1 - \omega_2)$ satisfies Equation (6) and $\tilde{f}(\omega)$ is the pulse Fourier transform. In deriving Equation (5), the frequency correlation of the PMD vector is used, which is given by [9, 13]:

$$E\{\Omega_i(\omega_1)\Omega_j(\omega_2)\} = \frac{1}{3}\delta_{ij}g(\omega_1 - \omega_2) = \delta_{ij}\frac{1 - \exp\left[-\frac{E\{\Delta\tau^2\}}{3}(\omega_1 - \omega_2)^2\right]}{(\omega_1 - \omega_2)^2} \quad (6)$$

For an unchirped Gaussian initial pulse with amplitude $f(t) = A \exp(-t^2/2T^2)$, where $T = \sqrt{2}\tau_o$ is the initial pulse width and A is the initial pulse amplitude, the broadening factor is calculated analytically and given by

$$b_{\text{unc}}^2 = 1 + x - \frac{1}{2}\left[\left(1 + \frac{4x}{3}\right)^{1/2} - 1\right] \quad (7)$$

where $x = E\{\Delta\tau^2\}/4\tau_o^2$ is a measure of the amount of average PMD relative to the pulse width. In the long-pulse regime ($x \ll 1$), the normalized broadening approaches $b_{\text{unc}}^2 \approx 1 + 2x/3$, while for $x \gg 1$ the PMD dominates the broadening and $b_{\text{unc}}^2 \approx x$.

PSP Transmission

The first approach to PMD compensation was based on launching the signal into a PSP, which results in less output signal distortion [14]. In practice, a control signal must be fed back to the input from the receiver. The analysis of such a system is performed considering $\mathbf{s} = \langle \mathbf{\Omega} \rangle / |\langle \mathbf{\Omega} \rangle|$ and the resulting average broadening becomes [12]:

$$b_{\text{psp}}^2 = 1 + x - \frac{3}{2}\left[\left(1 + \frac{4x}{3}\right)^{1/2} - 1\right] \quad (8)$$

which is always smaller than the uncompensated result. In particular, for small PMD values ($x \ll 1$), we have $b_{\text{psp}}^2 \approx 1 + x^2/3$. On the other hand, for large PMD values the squared broadening factor increases proportionally to x .

First-Order Compensation at the Carrier Frequency

One compensation approach in the receiver is to cancel out the PMD vector at the carrier frequency $\mathbf{\Omega}(0)$ with a variable first-order PMD compensator. The input PMD vector of such a system is the vector sum of the PMD vector of the fiber and that of the compensator; i.e., $\mathbf{\Omega}_{\text{tot},1} = \mathbf{\Omega} - \mathbf{\Omega}(0)$. The pulse broadening in this case can be calculated performing a similar analysis as above but now by using the vector $\mathbf{\Omega}_{\text{tot},1}$ instead of $\mathbf{\Omega}$. The result is [12]:

$$b_{\text{1st}}^2 = 1 + \frac{5x}{3} - \frac{1}{2}\left[\left(1 + \frac{4x}{3}\right)^{1/2} - 1\right] - 4\left[\left(1 + \frac{2x}{3}\right)^{1/2} - 1\right] \quad (9)$$

In Equation (9), b_{1st}^2 increases as $1 + x^2/3$ for small x , giving the same result as the PSP method. However, for large x , b_{1st}^2 increases as $5x/3$, which is actually worse than the uncompensated system. In fact, for x greater than 12, first-order compensation at the carrier frequency deteriorates the system performance relative to the uncompensated case.

Second-Order Compensation at the Carrier Frequency

In the second-order compensation at the carrier frequency, the total PMD vector is given by $\mathbf{\Omega}_{\text{tot},2} = \mathbf{\Omega} - \mathbf{\Omega}(0) - \mathbf{\Omega}^{(1)}(0)\omega$, where $\mathbf{\Omega}^{(1)}(0)$ denotes the first frequency derivative of the PMD vector at the carrier frequency. The broadening factor is calculated as in the previous cases [15]:

$$b_{2\text{nd}}^2 = b_{1\text{st}}^2 + \frac{x^2}{3} - 12 \left[\left(1 + \frac{2x}{3}\right)^{1/2} - \frac{x}{3} \left(1 + \frac{2x}{3}\right)^{-1/2} - 1 \right] \quad (10)$$

From Equation (10) it can be seen that $b_{2\text{nd}}^2$ increases as $1 + (8x^3/27)$ for small x , so that the PMD impairment is reduced further than the first-order compensation case. However, for large x , $b_{2\text{nd}}^2$ increases as $x^2/3$, which is actually much faster than the first-order compensation and the uncompensated cases.

In fact, the PMD compensation approach based on the Taylor's expansion of the fiber PMD vector up to a certain order at a specific frequency does not work for large PMD-to-pulse width ratios. In this case, the valid frequency range of the expansion is much narrower than the signal bandwidth, and thus, the higher-order terms in the expansion rather increase the error between the fiber PMD vector and the compensation vector over the signal bandwidth. Since the higher-order term grows faster, a larger error will be incurred as the order of the expansion increases.

Compensation with the Averaged PMD Vector

A better strategy is to use a compensating vector equal to the frequency average of the higher-order PMD vector of the fiber in emulating the PMD vector. The compensation PMD vector will be then in the form of $\mathbf{\Omega}_c = \langle \mathbf{\Omega} \rangle + \langle \mathbf{\Omega}^{(1)} \rangle \omega + \dots$

In the first-order compensation, the total PMD vector is $\mathbf{\Omega}_{1\text{st}} = \mathbf{\Omega} - \langle \mathbf{\Omega} \rangle$, and the broadening factor turns out to be exactly equal to that given by the PSP method:

$$b_{1\text{st}}^2 = 1 + x - \frac{3}{2} \left[\left(1 + \frac{4x}{3}\right)^{1/2} - 1 \right] \quad (11)$$

As observed previously, the squared broadening factor increases as $1 + x^2/3$ for small PMD values, while for large PMD values increases as x .

In the case of the second-order compensation, the total PMD vector becomes $\mathbf{\Omega}_{2\text{nd}} = \mathbf{\Omega} - \langle \mathbf{\Omega} \rangle - \langle \mathbf{\Omega}^{(1)} \rangle \omega$ and the broadening factor is [15]:

$$b_{2\text{nd}}^2 = b_{1\text{st}}^2 + \frac{3}{2} \left(1 + \frac{4x}{3}\right)^{3/2} - 3(x+1) \left(1 + \frac{4x}{3}\right)^{1/2} + \left(\frac{4x^2}{3} + 2x\right) \left(1 + \frac{4x}{3}\right)^{-1/2} + \frac{3}{2}. \quad (12)$$

From Equation (12) it can be seen that $b_{2\text{nd}}^2$ increases as $1 + (2x^3/9)$ for small x , so that the PMD impairment is reduced further than the first-order compensation case. On the other hand, for large x , $b_{2\text{nd}}^2$ increases as x . Therefore, the second-order compensation

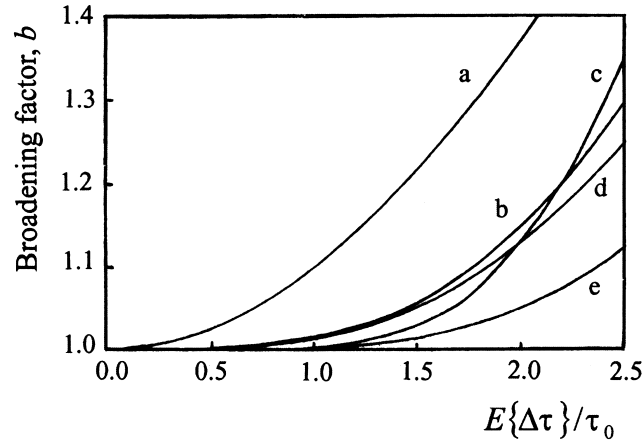


Figure 1. Average broadening factors, b , as a function of the normalized average DGD for the uncompensated case (a), for different compensation schemes: first-order PMD cancellation at the carrier frequency (b), second-order PMD cancellation at the carrier frequency (c), PSP or first-order cancellation of the average PMD vector (d), and second-order cancellation of the average PMD vector (e).

has smaller pulse broadening than the first-order compensation and the uncompensated cases for all PMD values.

We conclude from the above results that the frequency average approach improves the system performance even for large PMD-to-pulse width ratios. Furthermore, the second-order compensation provides a better performance than the first-order compensation for all PMD-to-pulse width ratios. However, as the PMD-to-pulse width ratio increases, the PMD compensation asymptotically reaches the same slope as the uncompensated case.

The system performance is expected to be improved further by choosing optimal compensation vectors rather than by using the frequency averages of the higher-order PMD vectors of the fiber as expansion coefficient vectors in compensation. For example, it was shown in [16] that the optimum first-order compensation vector is $\mathbf{\Omega}_c = \langle \mathbf{\Omega}_o \rangle + [\alpha^2 \langle \mathbf{s}_o \rangle / (1 - \langle \mathbf{s}_o \rangle^2)]$, where $\mathbf{\Omega}_o$ and \mathbf{s}_o are the output PMD vector and the output SOP, respectively, and $\alpha = \langle \mathbf{s}_o \rangle \cdot \langle \mathbf{\Omega}_o \rangle - \langle \mathbf{s}_o \cdot \mathbf{\Omega}_o \rangle$. The resulting squared broadening factor behaves as $1 + (x^2/9)$ for small PMD values, which represents an improvement compared to the case $\mathbf{\Omega}_c = \langle \mathbf{\Omega} \rangle$.

At the moment, a search for the expression of the optimum compensation vector for higher-order compensation remains as a topic of research. The above results suggest that the optimal coefficient vectors will be associated with the frequency average of the higher order PMD vectors rather than the higher order PMD vectors at a specific frequency.

Figure 1 illustrates the calculated broadening factors, obtained from Equations (7)–(12), as a function of the ratio of the PMD value to the initial rms pulse width, $E\{\Delta\tau\}/\tau_0 = \sqrt{32x/3\pi}$. It can be observed that in the case of second-order PMD compensation at the carrier frequency (curve c), the broadening factor increases rapidly and the system performance is deteriorated for large PMD-to-pulse width ratios. However, if the compensation is realized with the frequency averaged second-order PMD vector (curve e), the system performance is effectively improved for all values of the PMD-to-pulse width ratio.

PMD Measurement

Several different techniques have been developed to measure the PMD in single-mode fibers. These techniques are usually classified in two main groups: frequency domain and time domain. In the frequency domain, the techniques include the wavelength scanning method, the Jones matrix eigenanalysis, the interferometer method and the Poincaré arc [17, 18]. In the temporal domain we find the pulse delay and the polarization phase shift methods [18, 19]. Besides these transmission techniques, the PMD could also be derived in the time domain from the analyses of the Rayleigh or Fresnel backscattered signal from the fiber [20, 21].

The polarization phase shift technique has been widely adopted by the equipment manufacturer for polarization-mode dispersion characterization. The great advantage of this method resides in the similitude between this technique and the other one, named modulation phase shift, largely used for chromatic dispersion characterization. Therefore, the conjugation of these two techniques allows the integration on a single piece of equipment the measurement capacity to characterize attenuation, phase, group delay, chromatic dispersion, and PMD.

A wavelength scanning-based technique commonly used is the fixed analyzer method, which relies on the measurement of the spectral transmission through a polarizer-fiber-polarizer concatenation scheme. The transmission spectrum is analyzed either by counting the transmission extreme or by applying a Fourier analysis. If the last polarizer is changed by a polarimeter, information about the three normalized Stokes parameters is obtained, providing a full description of the output polarization, over wavelength. The mean DGD could be calculated from each one of these Stokes parameters. Using the three Stokes parameters, the measurement accuracy can be increased by means of averaging. The rate of rotation of the output state of polarization about the principal states axis is a measure of the differential group delay of the fiber. The mean DGD, $\langle \Delta\tau \rangle$, could be determined by counting the extremes of each Stokes parameter curve [18, 22].

$$\langle \Delta\tau \rangle = 0.824 \frac{N_e \lambda_{\text{start}} \lambda_{\text{end}}}{2(\lambda_{\text{start}} - \lambda_{\text{end}})c} \quad (13)$$

where λ_{start} and λ_{end} are the limits of the wavelength sweep, N_e represents the number of transmission extremes (peaks and valleys) that occur across the scan, and c is the speed of light in a vacuum. This expression is valid for measurement on fibers with a length longer than the beat length. In this situation we have $\frac{N_e}{N_m} \rightarrow 1.524$, where N_m is the number of crossings by the mean value (see [22]).

The measured standard deviation is given by:

$$\frac{\sigma}{\langle \Delta\tau \rangle} \approx \sqrt{\frac{0.5}{N_e}} \quad (14)$$

The fixed analyzer method (with polarimeter procedure) was applied to determine the DGD associated to a 20-km reel of single-mode (G.652) fiber. This procedure was then used to determine the mean DGD for other fiber lengths (45 and 70 km).

It was considered a 100-nm scanning interval (1500 to 1600 nm) with a 1 nm-wavelength step. The state of polarization at the fiber input was kept linear and constant along all the wavelength sweeping. Figure 2 shows the normalized Stokes parameters evolution obtained at the fiber output, represented over the Poincaré sphere. For better visualization, these parameters are represented in a bidimensional form in Figure 3.

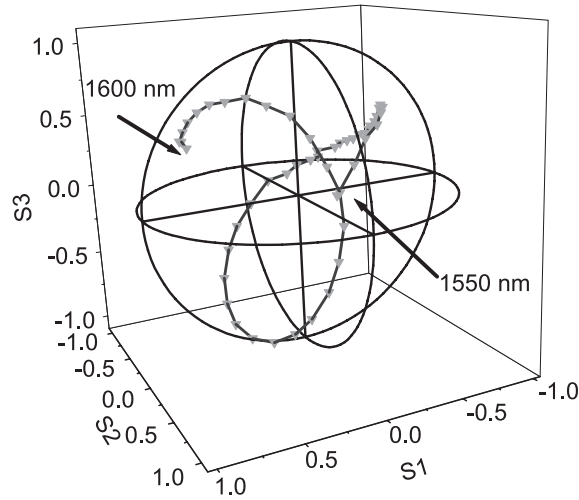


Figure 2. Stokes parameters evolution along 100-nm wavelength scanning represented over the Poincaré sphere for 20 km of G.652 fiber.

The situation previously analyzed fall in the long-length regime. Therefore, we can refer to expression (1) to obtain the DGD, leading to a value of 0.1382 ps with a standard deviation of 0.0250 ps. The same procedure was applied to other fiber lengths. Figure 4 illustrates the Stokes parameters evolution along 100-nm wavelength scanning for 70 km of G.652 fiber.

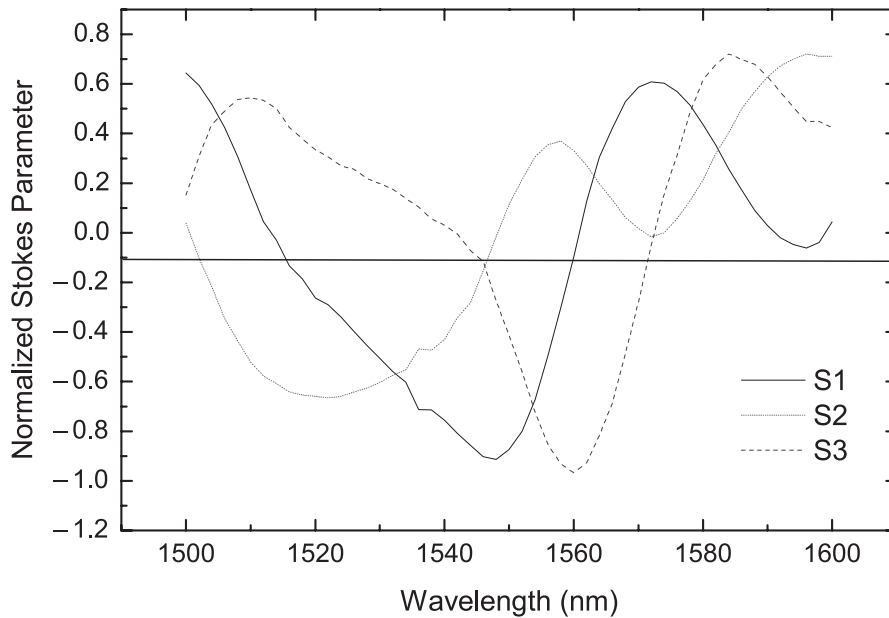


Figure 3. Stokes parameters evolution along 100-nm wavelength scanning for 20 km of G.652 fiber. For all the Stokes parameters we have: $N_e = 3$, $N_m = 2$, $N_e/N_m = 1.5$.

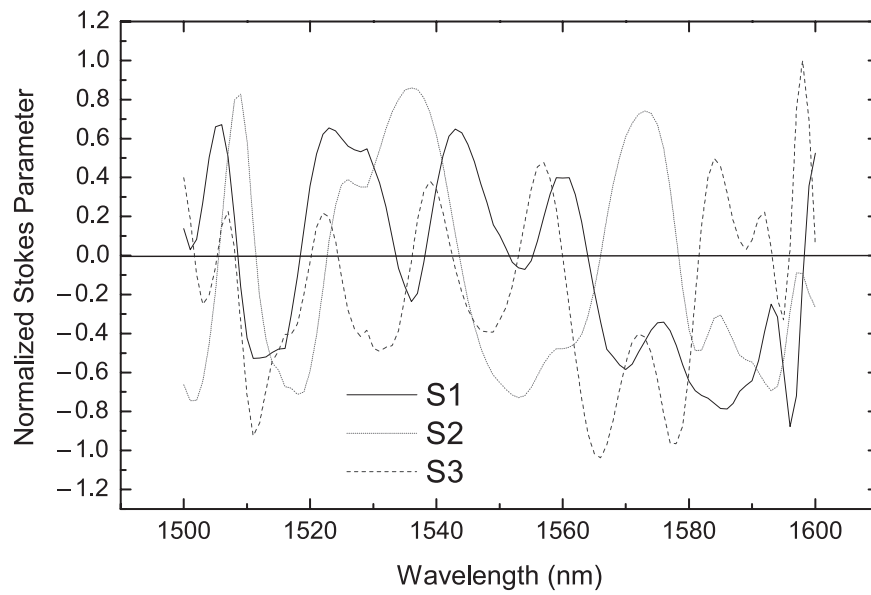


Figure 4. Stokes parameters for 70 km of G.652 fiber.

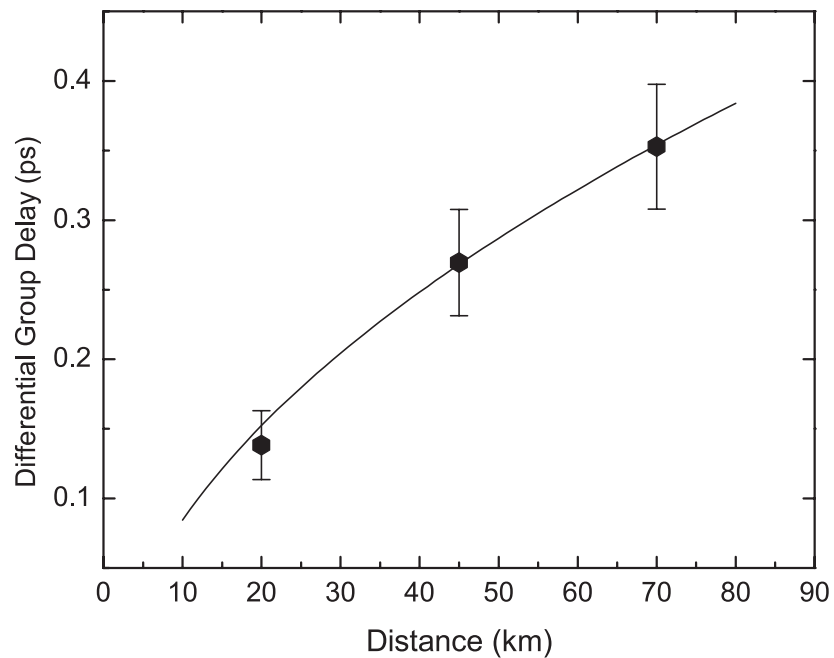


Figure 5. Mean DGD as functions of fiber length. Dots are experimental data, and the line is the data fit using expression (13).

The experimental values of the mean DGD were adjusted to a square root law (Figure 5), and a PMD coefficient of 0.0518 ± 0.0057 ps/ $\sqrt{\text{km}}$ was obtained.

PMD Emulation

The statistical nature of the PMD effect [6, 8, 9] makes difficult to assess the PMD compensators. If we use an installed communications system for this assessment we will need to wait very long times to evaluate the emulator over a significant range of DGD values. An accurate assessment of PMD compensators is only possible with a PMD emulator system that presents the same PMD properties of the link and that could quickly cycle through different DGD values. A PMD emulator make possible a fast and versatile access to all possible DGD values, especially DGD values with low probability. Nevertheless the statistics of PMD produced by an emulator should be related, in a known way, with the real fiber statistics.

A Maxwellian pdf (see Equation (2)) of DGD is the first key performance that a PMD emulator should meet. The emulator should also produce accurate higher-order PMD statistics, at least up to the second order. Another aspect to consider is the PMD autocorrelation function (ACF). This function presents a theoretical quadratic decay with $\Delta\omega$ (see Equation (6)), and this is another important performance that a PMD emulator should meet. Ideally, the residual correlation should have values less than 10% for all frequencies outside of a 0.2 nm bandwidth. On the other hand, to act as a practical measurement tool, a PMD emulator should also exhibit features like stability, repeatability, predictability, and simplicity.

Emulator Types

A real fiber is usually modeled by the concatenation of randomly coupled linear birefringence sections. In the same way, a device to emulate fiber PMD may be constructed by the concatenation of several birefringence elements [23]. These birefringence elements may be sections of polarization maintaining fiber (PMF), birefringence crystals, or other devices that provide a differential group delay between the two orthogonal polarization axes.

The main PMD emulators can be classified in to one of the five main emulator types:

Emulators with Fixed Orientation Sections

The PMD emulators with fixed orientations may be constructed by the concatenation of several number of PMF sections [24, 25] spliced at fixed angles. A rigorous statistic analysis of his results was only made theoretically. A computational simulation [24] of an emulator with 15 equal length PMF sections, spliced randomly, generated a DGD distribution well described by a Maxwellian distribution over an ensemble of frequencies. However, these emulator types have strong limitations since only with wide varying wavelength is it possible to obtain different PMD emulator states.

Emulators with Uniform Scattering of Polarization

This emulator type consists of placing polarization scramblers between the PMF sections to uniformly scatter the polarization state over the Poincaré sphere. The uniform scatter of the polarization is easy to model in a computer but hard to realize in practice where

polarizations controllers are used. Simulation results of three different emulators, each one with different number (three, five, and ten) of randomly PMF sections length, were compared in [26]. The results showed that only with ten or more PMF sections is the pdf of DGD well fitted by a Maxwellian distribution.

Emulators with Rotatable Sections

In emulators with rotatable sections, the birefringence sections randomly rotate relative to each other. Damask [27] constructed an emulator consisting of twelve equal-length yttrium ortho-vanadate (YVO₄) birefringence crystals mounted with twelve independent and motorized rotation stages placed in cascade. First- and second-order PMD have been well generated. However, all moving parts can affect emulator features like stability or repeatability.

Two PMD emulators, with 3 and 15 PMF sections connected with rotatable connectors, have also been constructed [28]. This technique makes it possible to easily generate different fibers realizations, at any specific wavelength, by randomly rotating the connectors. The results show that only with 15 PMF sections the emulator has DGD values in good agreement with the Maxwellian distribution. The 15 PMF sections emulator also exhibits good results in the autocorrelation function ACF of the PMD vector.

Emulators with Tunable Birefringence

Although there are reasonable results exhibited by the last two emulator types, they still present some issues like cumbersome, relatively high losses or an insufficient automatic control. An emulator with tunable birefringence sections, exploiting the temperature sensitivity of PMF, was presented in [29]. This emulator exhibited reasonable results: first-order PMD was well fitted with a Maxwellian distribution and measured second-order PMD only differs from expected theoretical distribution in the low probability tail. The ACF had higher residual correlation value (20%) comparatively with the 15 PMF sections connected with rotatable connectors emulator described above that have only 10% of residual correlation. A possible way to solve these two issues is to increase the number of PMF sections. The main advantages of this compact emulator over other emulators are low loss, electrically controllable, no moving parts, negligible polarization-dependent loss (PDL), and no internal reflections.

Emulators with Tunable Statistics

An emulator with tunable statistics presented by [30] makes use of three programmable DGD elements separated by two fiber-squeezer-based polarization controllers. The DGD elements consist of several birefringence crystals whose lengths increase in a binary series separated by electrically driven polarization switches and can be programmed to generate any desired DGD value [31]. Varying the DGD of each element according to a Maxwellian distribution with average $\langle \Delta\tau \rangle$ and uniformly scattering the polarization between sections, a Maxwellian distribution with average $3^{1/2}\langle \Delta\tau \rangle$ is yielded at the emulator output. The experimental results show a possibility of accurately tuned PMD statistics. The first-order PMD values are well fitted by a Maxwellian; however, the mean of second-order PMD is about 30% lower than expected for a real fiber. Simulation results reveal that with only fifteen or more DGD elements is possible to obtain an ACF with residual correlation values lower than 10% [32]. Features like stability and repeatability

are well achieved. Another advantage of this emulator is the possibility to experimentally generate extremely low probability events, allowing the powerful technique of importance sample to be applied.

An Emulator Based on Nonlinear Chirped FBGs

At the present we are developing a programmable group delay module using two nonlinear chirped fiber Bragg gratings (FBGs) written into a high-birefringence fiber (hibi). The large refraction index difference present in the hibi fiber makes with the Bragg refraction from the chirped grating, for a given signal wavelength occurring at different locations for different polarizations. The two signal polarizations “see” two different gratings due to the birefringence. The position difference of the reflection produces a differential time delay between the two polarizations, corresponding to first-order PMD [33].

The proposed architecture for our module is shown in Figure 6. The key elements are the two polarization controllers (PC1 and PC2) and the two nonlinear chirped FBGs (hibi FBG1 and hibi FBG2) written into a hibi fiber. The input signal enters in the PC1 in order to obtain a state of polarization parallel to the fast birefringence axis of hibi FBG1. The PC2 ensure a correct coupling between the fast birefringence axis of hibi FBG1 and the slow birefringence axis of hibi FBG2. In this configuration the two DGDs generated at each grating are subtracted.

The DGD corresponding to hibi FBG1 has a constant value $\Delta\tau_1$ ps and that corresponding to hibi FBG2, has a tunable value $\Delta\tau_2(V)$ ps. It can be continuously varied by mounting the hibi FBG2 on a voltage-controlled piezoelectric element. The mechanical stretching should induce a variation in the DGD between the two polarizations. If no voltage is applied to hibi FBG2 $\Delta\tau_2$ has the same value as hibi FBG1 ($\Delta\tau_2(V=0) = \Delta\tau_1$), and in case of maximum voltage applied (related with the maximum stretch grating support) hibi FBG2 has the value $\Delta\tau_2(v^m) = \Delta\tau_2^m$. The total DGD generated by this module, $\Delta\tau_t$, could take values from 0 to $(\Delta\tau_2^m - \Delta\tau_1)$ ps.

The precise and repeatable DGD generation capability of our DGD module will be related with the rigorous parameters calibration of the curve $\Delta\tau_2(V)$, which describes the DGD variation with applied voltage. To any applied voltage in hibi FBG2 it should

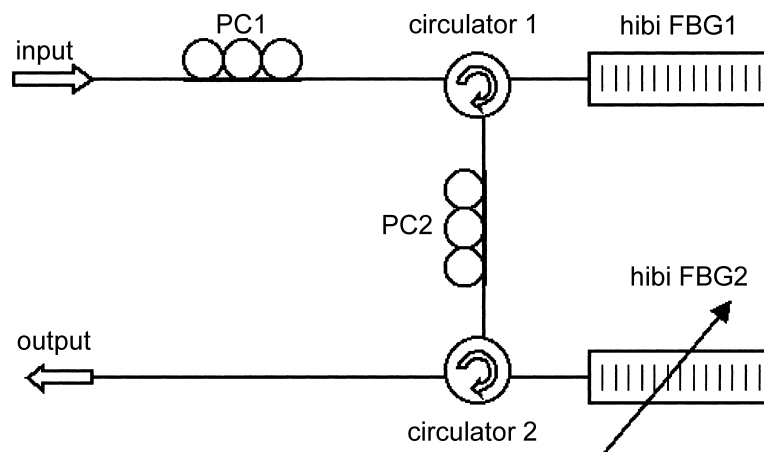


Figure 6. Schematic diagram of the group delay module using two nonlinear chirped FBGs written into a hibi fiber.

correspond to a deterministically $\Delta\tau_2(V)$ value and a respective $\Delta\tau_t$ at the module output. Eventual environmental perturbations, like temperature variation, will induce time delay variations in both gratings, which means that the difference between them remains constant. Developing the software tools necessary to control the DGD module should make it possible to use to generate statistical DGD samples with a Maxwellian distribution and a selectable average. By the concatenation of several modules like this separated by polarization scatter, it should be possible to emulate second-order PMD.

PMD Compensation with an Electrical Equalizer

Electronic equalization is a well-established technique largely used in automatic phone line equalization [34]. These same principles can also be applied to high-speed lightwave transmission systems. Electronic dispersion compensation (EDC) has been reported to overcome fiber dispersion in metro links [35]. Electrical filter-based devices are now under deep study and are expected to have a significant impact at the high bit rate optical link receiving edge. These devices are in general based on analog domain transversal filters that are able to operate at higher bit rate signals (10 Gbit/s, 40 Gbit/s and potentially above) [36, 37]. A major advantage of EDC is the possibility of electronic adjustment, making it in principle possible to compensate for changes in receiver response or other distortions due to ageing and/or temperature variations.

Inter symbol interference (ISI), due to chromatic dispersion (CD) and polarization mode dispersion (PMD) are major impairments that affect pulse shape in high-speed systems and should be mitigated. Monolithic microwave integrated circuit (MMIC) techniques allow the realization of high-performance, reliable microwave circuits and are thus suitable for implementation as filters in current high bit rate electro-optical transceivers. The introduction of electrical noise can be stated as the main counter back when using EDC in optical channel equalization.

Simple Electrical Equalizer Model

Figure 7 shows a simple Transversal Filter (TF) model. In the Synchronously Spaced Equalizer (SSE) the incoming signal is delayed by one bit period per stage, while in the Fractionally Spaced Equalizer (FSE) the delay is less than one bit period. For high speed systems the FSE is best choice in order to avoid aliasing in the equalized signal [38]. Both configurations are known as feed-forward equalizers (FFE).

The incoming signal is next tapped and weighted by stage coefficients, c_n , that can adaptively be changed so that the resulting filter response equals as much as possible the inverse of the channel response.

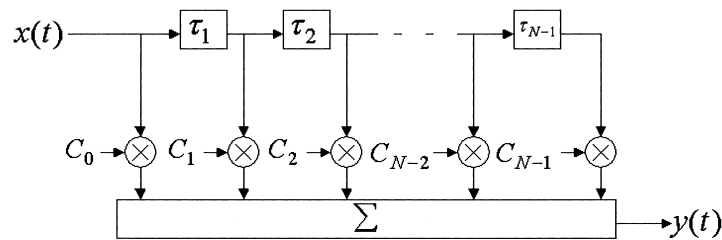


Figure 7. Simple transversal filter (TF) model.

A 10 Gb/s SiGe IC FFE comprising eight taps, aiming to compensate over 95 km of standard single-mode fiber (SMF) was already tested [39]. Full DGD compensation was reported for values up to 65 ps, while 3.4 dB of gain penalty reductions were measured for DGD of 100 ps.

Recent studies on this topic show that some other filter structures derived from the TF, namely the decision feedback equalizer (DFE), are capable of improving EDC circuit performances. The DFEs are nonlinear filters that are able to cope with severe signal distortions. This device gathers its knowledge from the previously detected bits and adjusts the level on the decision block by subtracting the previous ISI from the decision to be made. Series combination of FFE-DFE structures outperforms single FFE and DFE electrical blocks, leading to an optimized operation [40].

For a 40 Gb/s systems, Nakamura [41] has recently reported for a 3 tap FFE-DFE IC using InP/InGaAs HBT technology achieving 20 ps of DGD mitigation.

For the automatic change of the filter coefficients, zero-forcing (ZF), least mean square (LMS) or other annealing techniques such as Metropolis algorithm annealing can be fast enough to set coefficients value while monitoring received pulse shape. They are effective with FFE, DFE, or even FFE-DFE structures.

Other digital equalizing processes like maximum likelihood sequence (MLS) analyzers are very robust for low data rate processing equalization [42]. Simplified versions of its analog implementation are beginning to be used in high bit rate systems [40, 43].

PMD Mitigation

In this study we will only account for first-order PMD. Looking forward to establish the EDC capabilities on PMD compensation, a numerical simulation was done, where an FFE device with 5 coefficients and a tap delay equal to one third of the incoming bit rate was considered after the photo-detector in the optical receiver. For coefficients automatic updating, a simplex algorithm with the eye-opening height as state variable was used [44].

In this work we numerically studied systems at two different bit rates, 10 and 40 Gb/s. In order to numerically consider the DGD, the signal is split and forced to follow two distinct paths. The propagation time difference between the paths is given by $\Delta\tau$, which models the time difference between the fast and slow polarization axis. Due to the random nature of the birefringence along the fiber, $\Delta\tau$ increases proportionally to the fiber length square root. The γ parameter governs the splitting process of the optical power between both arms (see Figure 8).

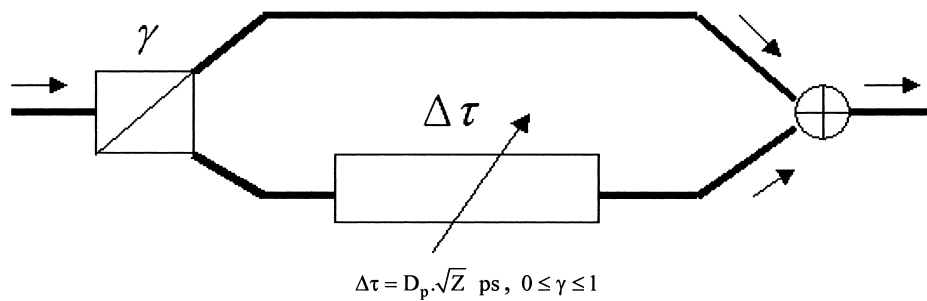


Figure 8. First-order PMD numerical emulator.

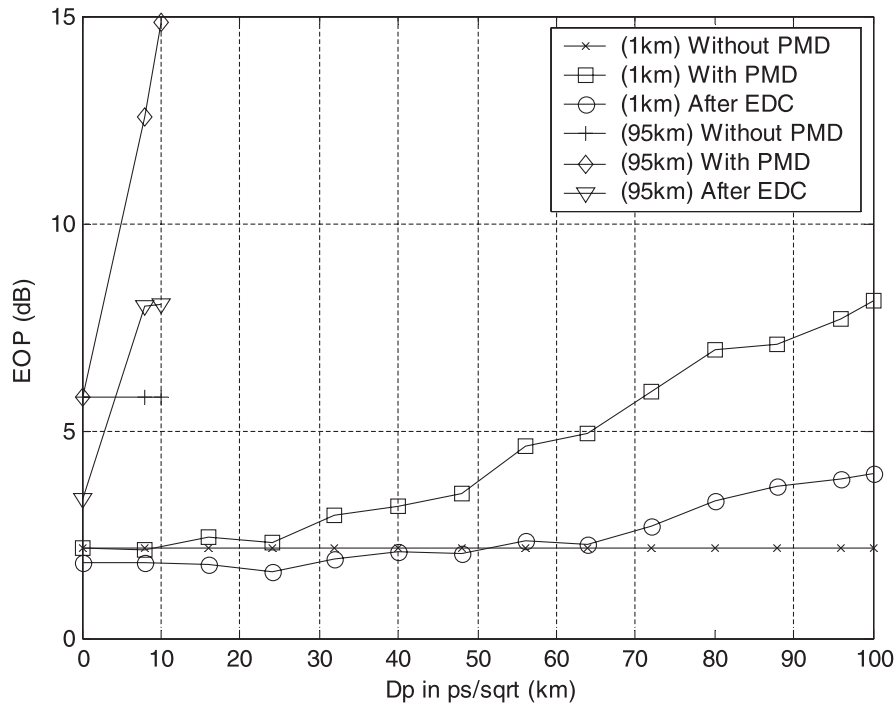
The fiber transfer function, given by

$$H_{\text{fiber}}(f) = \exp\left(j \frac{\pi DL\lambda^2 f^2}{c}\right) \quad (15)$$

was implemented in both arms of the emulator of Figure 8. In Equation (15) the product DL states for the total chromatic dispersion in ps/nm, D being the dispersion and L the total length of the system. We considered several distances and in all cases we assumed $D = 17$ ps/nm/km.

The output optical signal is then amplified to completely compensate for the optical losses. Amplification spontaneous emission (ASE) noise is added to the signal leading to an optical signal-to-noise ratio (OSNR) at the receiver input of 13 dB, measured over 0.1 nm and 0.34 nm of optical bandwidth for 10 Gbit/s and 40 Gbit/s rates, correspondingly. After photo-detection, modeled as a square law device, adaptive EDC is finally performed. An electrical noise factor of 10 dB for the EDC filter was considered.

The splitting ratio, γ , is the relative power traveling in the fast axis, while slow axis optical signal is delayed by $\Delta\tau$ (ps). When γ equals one, we have all-optical power traveling through the fast axis. By the opposite way, when γ equals zero, all-optical power is considered to travel through the slow axis. A ratio for fast to slow axis relative power of 0.7/0.3 or even 0.5/0.5 are usually stated, giving this last ratio the worst overall power penalty.



(a)

Figure 9. EDC numerical results for a 512 bits NRZ PRBS over an SMF link. The splitting ratio considered in the numerical PMD emulator was 0.7. Figure 9a refers to a 10 Gbit/s system.

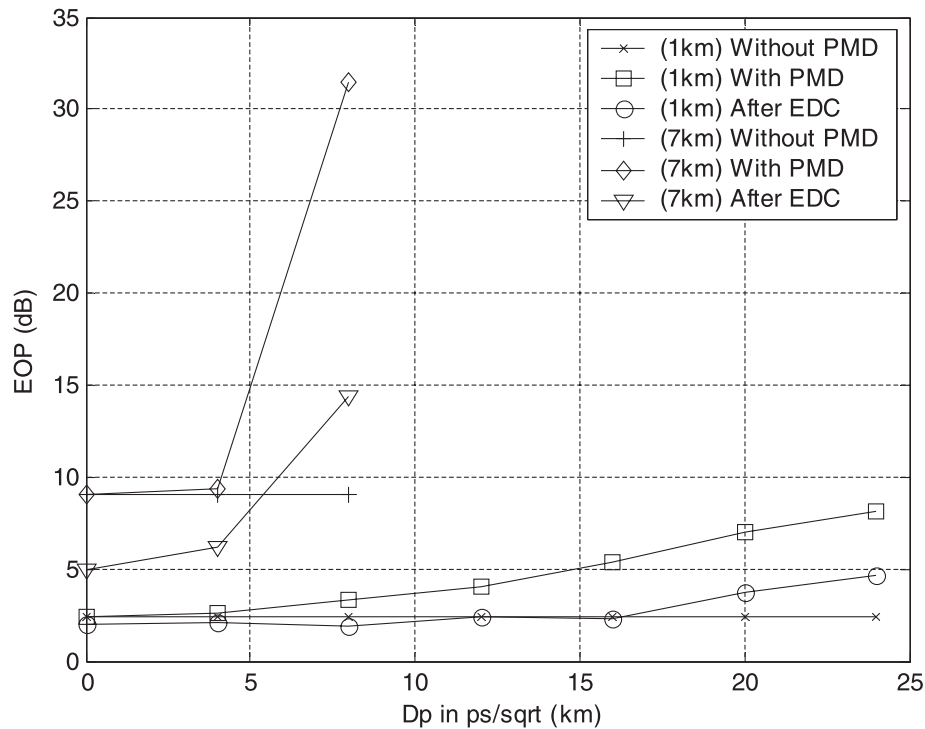
Since signal quality evaluation methods, based on the Q-factor, are not so reliable when strong ISI is present, an eye-opening penalty (EOP) ratio was defined by

$$\text{EOP} = -10 \cdot \log \left(\frac{H}{H_{\text{ref}}} \right) \text{ (dB)} \quad (16)$$

where H_{ref} states for the eye-opening in a back-to-back configuration and H is the eye-opening measured after the signal had crossed the link.

Simulations were carried out for two different scenarios. The first scenario, “without PMD,” means considering only the CD in the link. In the second scenario, “with PMD,” CD and PMD were both considered. The first scenario is used as a reference point. Systems operating at 10 and 40 Gb/s were simulated and the results are presented in Figure 9.

By looking at Figure 9a we see that FFE is able to fully compensate for roughly 65 ps of DGD for a 10 Gb/s SMF link while showing an EOP improvement of 4 dB at 100 ps of DGD. These results are quite similar to those reported by Ceriali et al. [39]. In Figure 9b, analogous results are presented for a 40 Gb/s link. In this case, 16 ps of DGD are fully compensated while achieving 4 dB of improvement in the EOP for 24 ps DGD after 1 km of SMF. In extreme signal detection conditions, after 7 km of SMF at 40 Gb/s, we may also see that an EOP improvement of 16 dB is theoretically possible



(b)

Figure 9. EDC numerical results for a 512 bits NRZ PRBS over an SMF link. The splitting ratio considered in the numerical PMD emulator was 0.7. Figure 9b to a 40 Gbit/s system.

for a 21 ps DGD. Nevertheless, in practice, difficult signal detection may be experienced with such a high level of impairment.

Dynamic Optical PMD Compensation

The dynamic PMD compensation in the optical domain is always based on the same principle: inducing a relative delay of one transversal polarization component of the fundamental propagation mode in relation to the orthogonal one. One of the approaches for optical PMD compensation is based on free-space optics [45]. The idea is to separate the two polarization components by a polarization-beam splitter in free-space optics. Before getting combined again in the fiber, each polarization component travels a different path, which induces different delays for each one. The tuning process is made by changing one of the optical paths. However, this method has all the inherent difficulties of free-space optics such as alignments or reflections. Other approaches use the temperature tuning of small lengths of highly birefringent (hibi) fibers [46], but the process lacks speed and flexibility.

One of the most promising techniques for dynamic compensation of the PMD is using chirped fiber Bragg gratings (CFBG) written in hibi fibers. In these fibers, the x - and y -components of the degenerated LP_{01} mode have different refractive indexes. Therefore, a hibi FBG will reflect two different wavelengths with orthogonal polarization. The wavelength difference between the two peaks is dependent on the birefringence of the fiber (B) and can be given by

$$\Delta\lambda_{\text{HB}} = 2B\Lambda \quad (17)$$

If the grating has a nonlinear chirp [47], the group delay is composed of two parabolic functions (one for each polarization) shifted by $\Delta\lambda_{\text{HB}}$. If the grating is tuned by temperature or longitudinal stress, the relative induced delay between the orthogonal polarizations for a specific wavelength will change. Figure 10 shows a simulation of a quadratic CFBG written in a hibi fiber with a birefringence of $B = 5 \times 10^{-4}$ where two different relative delays can be observed at 1550 nm, just by tuning the grating.

In a linear CFBG written in a hibi fiber, each position in the grating will reflect two wavelengths at orthogonal polarizations. This means that the group delay of these gratings is a combination of two linear functions, one for each polarization, with the same slope (m) and shifted by $\Delta\lambda_{\text{HB}}$:

$$\begin{aligned} \tau_y(\lambda) &= m\lambda + b \\ \tau_x(\lambda) &= m(\lambda - \Delta\lambda_{\text{HB}}) + b \end{aligned} \quad (18)$$

Here, it is assumed that the y polarization is the fast axis, so the reflection spectrum corresponding to y polarization is at lower wavelengths than the one corresponding to x polarization. So, the relative group delay induced by a linear CFBG written in a hibi fiber ($\Delta\tau = \tau_x - \tau_y$) is calculated as

$$\begin{aligned} \Delta\tau &= -m\Delta\lambda_{\text{HB}} \\ &= -2mB\Lambda \end{aligned} \quad (19)$$

Expression (19) shows that the dynamic tuning of the induced PMD can be made by adjusting the birefringence of the fiber [48] or by adjusting the dispersion slope of the grating.

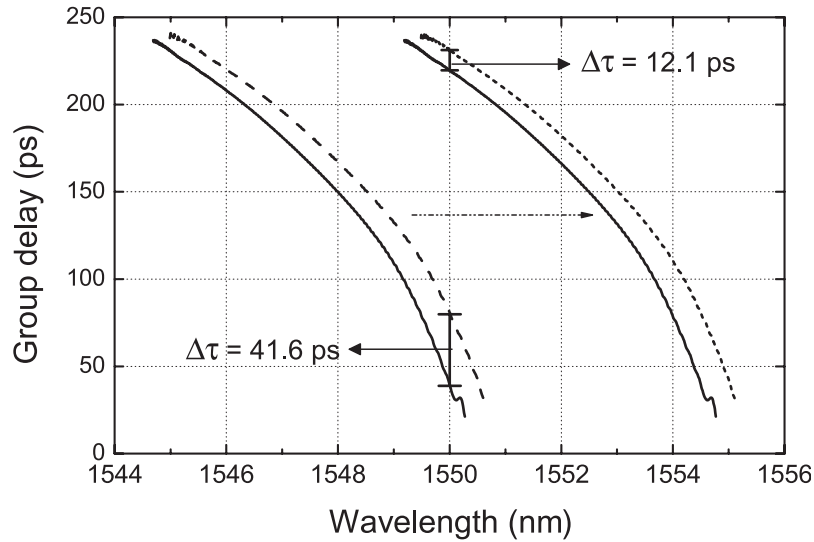


Figure 10. Group delay of a quadratic CFBG written in a hibi fiber for different central wavelengths. Solid: y polarization; dashed: x polarization.

Experimental Results

Since a linear CFBG is easier to write, we have developed a tunable PMD compensator based on dynamic tuning of the dispersion slope. A uniform fiber Bragg grating was written in a hibi fiber with 24 mm length using a scanning beam from an Ar-ion laser frequency doubled by a BBO crystal to 244 nm. The grating was inserted in a zinc substrate, which has a high thermal resistance. On each side of the Zn channel, a peltier forces a constant temperature. With this, different temperature gradients can be achieved by changing the individual temperatures on the peltiers. The grating was isolated from the air to avoid temperature deviations and heat loss due to convection. Since the substrate has a constant width and height along its length, the temperature gradient is linear; therefore, it induces a linear chirp on the grating, which depends on the difference of temperature, ΔT , between the two peltiers. Figure 11 shows the reflection spectra of the grating under different temperature gradients.

The spectrum broadening due to the induced chirp as the temperature difference increases is quite visible. At $\Delta T = 10^\circ\text{C}$, the two peaks at orthogonal polarizations are still separated. When ΔT is increased to $\Delta T = 30^\circ\text{C}$ the two peaks are starting to overlap. The delay between x and y polarizations can be tuned for any wavelength in the overlap region by adjusting the dispersion slope (which depends on ΔT). The group delay between the two orthogonal polarizations, at 1544.75 nm, was measured for different temperature differences. The results are displayed in Figure 12.

The group delay between the two orthogonal polarizations was tuned between -35 to 110 ps for temperature gradients between 0 and 50°C , respectively. After $\Delta T = 10^\circ\text{C}$, the two orthogonal peaks start to overlap, increasing the group delay between x and y polarizations. It is also possible to see that the evolution is quite linear with the temperature gradient increase, which simplifies the implementation in a prototype with feedback architectures. The results show that it is possible to compensate the PMD with an induced temperature gradient in a uniform fiber Bragg grating written in a hibi fiber.

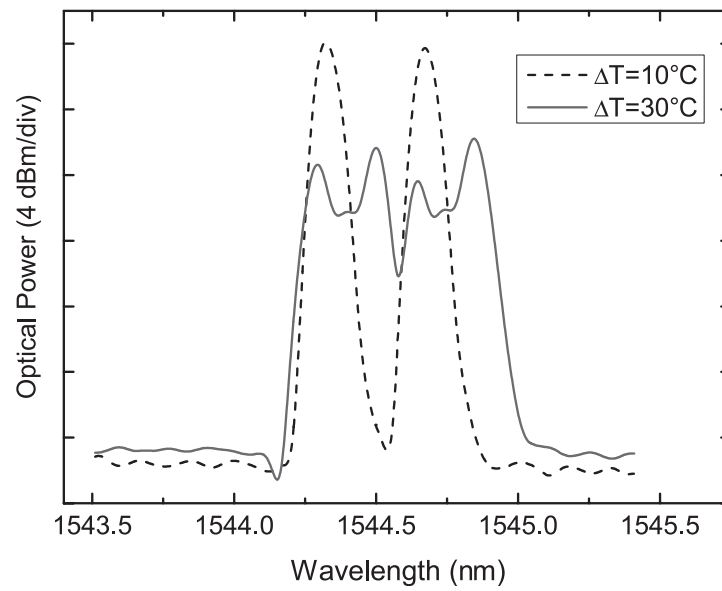


Figure 11. Reflection spectra of an FBG written in a hibi fiber with two induced temperature gradients: $\Delta T = 10^\circ\text{C}$ and $\Delta T = 30^\circ\text{C}$.

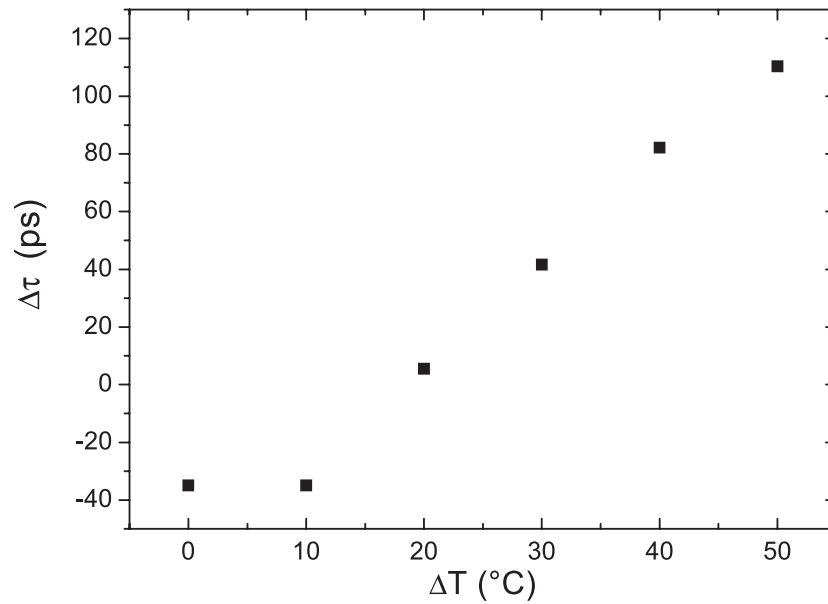


Figure 12. Difference in group delay between the two orthogonal polarizations for different applied temperature gradients.

Conclusions

In this article we presented a review of recent research related to polarization-mode dispersion in high-speed fiber-optic transmission systems. The basic theory of PMD, as well as some PMD compensation methods, were analyzed and compared, considering particularly the issue of pulse broadening. The problem of PMD measurement was discussed and some results obtained using the fixed analyzer method were presented. Due to the statistical nature of PMD, it is difficult to assess the performance of a PMD compensator in a real fiber communication system. A PMD emulator makes possible such assessment and a review of the main PMD emulator types was presented. Moreover, a novel emulator was proposed based on two nonlinear chirped fiber Bragg gratings written into a high-birefringence (hibi) fiber. Some PMD compensation techniques were reviewed and discussed. In particular, an electrical equalizer able to adaptively compensate up to 65 ps and 16 ps of DGD for 10 Gb/s and 40 Gb/s, respectively, was described. Improved performances may be expected as advanced high-speed electronic processing techniques become available. Dynamical optical compensation using chirped fiber Bragg gratings written in high-birefringence fibers was also demonstrated. The obtained experimental results show that it is possible to compensate the PMD with an induced temperature gradient in a uniform fiber Bragg grating written in a hibi fiber.

Acknowledgments

This work was partially supported by Fundação para a Ciência e Tecnologia (FCT) of Portugal, FEDER and POSI, within project POSI/CPS/47389/2002, “PMD—Polarization Mode Dispersion in High-Speed Optical Communication Systems” and by the Portuguese ADI—Agência de Inovação, in the context of the “The Most-Transimpedance Highly Efficient Micro&milimetrowave Optical Smart Transceiver” project. M. H. Sousa acknowledges support from the Fundação para a Ciência e a Tecnologia (FCT) of Portugal through a Doctoral Fellowship (SFRH/BD/1325/2000).

References

1. Matera, F., M. Settembre, M. Tamburrini, F. Favre, D. Le Guen, T. Georges, M. Henry, G. Michaud, P. Franco, A. Shiffini, M. Romagnoli, M. Guglielmucci, and S. Casceli. 1999. Field demonstration of 40 Gb/s soliton transmission with alternate polarizations. *J. Lightwave Technol.* 17:2225–2234.
2. Kolltveit, E., P. A. Andrekson, J. Brentel, B. E. Olsson, B. Bakhshi, J. Hansryd, P. O. Hedekvist, M. Karlsson, H. Sunnerud, and J. Li. 1999. Single wavelength 40 Gb/s soliton field transmission experiment over 400 km of installed fiber. *Electron. Lett.* 35:75–76.
3. Sunnerud, H., M. Karlsson, C. Xie, and P. A. Andrekson. 2002. Polarization-mode dispersion in high-speed fiber-optic transmission systems. *J. Lightwave Technol.* 20:2204–2219.
4. Poole, C. D., and J. Nagel. 1997. Polarization effects in lightwave systems. In *Optical Fiber Telecommunications IIIa*, edited by I. P. Kaminow and T. L. Koch. San Diego: Academic.
5. Poole, C. D., and R. E. Wagner. 1986. Phenomenological approach to polarization dispersion in long single-mode fibers. *Electron. Lett.* 22:1029–1030.
6. Foschini, G. J., and C. D. Poole. 1991. Statistical theory of polarization dispersion in single mode fibers. *J. Lightwave Technol.* 9:1439–1456.
7. Curti, F., B. Daino, Q. Mão, F. Matera, and G. Someda. 1989. Concatenation of polarization dispersion in single-mode fibers. *Electron. Lett.* 25:290–292.
8. Poole, C. D. 1991. Statistical treatment of polarization dispersion in single-mode fibers. *Opt. Lett.* 13:687–689.

9. Karlsson, M., and J. Bredel. 1999. Autocorrelation function of the polarization mode dispersion vector. *Opt. Lett.* 24:939–941.
10. Kogelnik, H., R. M. Jopson, and L. E. Nelson. 2002. Polarization mode dispersion. In *Optical Fiber Telecommunications IVb*, edited by I. P. Kaminow and T. Li. San Diego: Academic.
11. Karlsson, M. 1998. Polarization mode dispersion-induced pulse broadening in optical fibers. *Opt. Lett.* 23:688–690.
12. Sunnerud, H., M. Karlsson, and P. A. Andrekson. 2000. Analytical theory for PMD-compensation. *IEEE Photon. Technol. Lett.* 12:50–52.
13. Lin, Q., and G. P. Agrawal. 2003. Correlation theory of polarization mode dispersion in optical fibers. *J. Opt. Soc. Am. B.* 20:292–301.
14. Ono, T., S. Yamazaki, H. Shimizu, and H. Emura. 1994. Polarization control method for suppressing polarization-mode dispersion in optical transmission systems. *J. Lightwave Technol.* 12:891–898.
15. Kim, S. 2002. Analytical theory of pulse broadening in optical higher-order PMD compensation. *J. Lightwave Technol.* 20:1118–1123.
16. Sunnerud, H., C. Xie, M. Karlsson, R. Samuelsson, and P. A. Adrekson. 2002. A comparison between different PMD compensation techniques. *J. Lightwave Technol.* 20:368–378.
17. Heffner, B. L. 1992. Automated measurement of polarization mode dispersion using Jones matrix eigenanalysis. *IEEE Photon. Tech. Lett.* 4:1066–1069.
18. Derickson, D., ed. 1998. *Fiber Optic Test and Measurement*. New Jersey: Prentice Hall.
19. Nelson, L. E., R. M. Jopson, H. Kogelnik, and J. P. Gordon. 2000. Measurement of polarization mode dispersion vectors using the polarization-dependent signal delay methods. *Optics Express.* 6:158–167.
20. Corsi, F., A. Galtarossa, L. Palmieiri, M. Schiano, and T. Tambosso. 1999. Continuous wave backreflection measurement of polarization mode dispersion. *IEEE Photon. Tech. Lett.* 11:451–453.
21. Sunnerud, H., B. Olsson, M. Karlsson, P. Andrekson, and J. Brentel. 2000. Polarization mode dispersion measurements along installed optical fibers using gated backscattered light and a polarimeter. *J. Lightwave Tech.* 18:897–904.
22. Poole, C., and D. Favin. 1994. Polarization mode dispersion measurements based on transmission spectra through a polarizer. *J. Lightwave Tech.* 12:917–929.
23. Willner, A., and M. Hauer. 2002. PMD emulation, *Venice Summer School on Polarization Mode Dispersion*.
24. Lima, I., R. Khosravani, P. Ebrahimi, E. Ibragimov, C. R. Menyuk, and A. E. Willner. 2001. Comparison of polarization mode dispersion emulators. *J. Lightwave Tech.* 19:1872–1881.
25. Prola, C., J. Silva, A. Forno, R. Passy, J. Weid, and N. Gisin. 1997. PMD emulators and signal distortion in 2.48-Gb/s IM-DD lightwave systems. *IEEE Photon. Techn. Lett.* 9:842–844.
26. Djupsjöbacka, A. 2001. On differential group-delay statistics for polarization-mode dispersion emulators. *J. Lightwave Techn.* 19:285–290.
27. Damask, J. 2000. A programmable polarization-mode dispersion emulator for systematic testing of 10 Gb/s PMD compensators. *Optical Fiber Communications (OFC) Conference*, Baltimore, Paper ThB3–1, 28–30.
28. Khosravani R., I. T. Lima Jr., P. Ebrahimi, E. Ibragimov, A. E. Willner, and C. R. Menyuk. 2001. Time and frequency domain characteristics of polarization-mode dispersion emulators. *IEEE Photon. Tech. Letters* 13:127–129.
29. Hauer M., Q. Yu, E. Lyons, C. Lin, A. Au, H. Lee, and A. Willner. 2004. Electrically controllable all-fiber PMD emulator using a compact array of thin-film microheaters. *J. Lightwave Tech.* 22:1059–1065.
30. Yan, L., M. Hauer, Y. Shi, X. Yao, P. Ebrahimi, Y. Wang, A. Willner, and W. Kath. 2004. Polarization-mode-dispersion emulator using variable differential-group-delay (DGD) elements and its use for experimental importance sampling. *J. Lightwave Tech.* 22:1051–1058.

31. Yan, L., C. The, G. Yang, L. Lin, Z. Chen, Y. Q. Shi, A. Willner, and X. Yao. 2003. Programmable group-delay module using binary polarization switching. *J. Lightwave Tech.* 21:1676–1684.
32. Lee H., M. Kim, and Y. Chung. 2003. Statistical PMD emulator using variable DGD elements. *IEEE Photon. Tech. Lett.* 15:54–56.
33. Lee, S., R. Khosravani, J. Peng, V. Grubsky, D. Starodutov, A. Willner, and J. Feinberg. 1999. Adjustable compensation of polarization mode dispersion using high-birefringence nonlinearly chirped fiber Bragg grating. *IEEE Photon. Tech. Lett.* 11:1277–1279.
34. Qureshi, S. 1982. Adaptive equalization. *IEEE Comm. Mag.* 20:9–16.
35. Winters, J., and R. Gitlin. 1990. Electrical signal processing techniques in long-haul fiber-optic systems. *IEEE Trans. Comm.* 38:1439–1453.
36. Monteiro, P., A. Borjak, F. da Rocha, J. J. O'Reilly, and I. Darwazeh. 1998. 10 Gbit/s pulse shaping distributed-based transversal filter front-end for optical soliton receivers. *IEEE Microwave and Guided Wave Letters* 8:4–6.
37. Monteiro, P., R. Ribeiro, M. Violas, and J. Rocha. 2001. 40 Gbit/s GaAs MMIC signal processor for optical communication systems. *Optical Fiber Communications (OFC) Conference*, Baltimore, Paper ThB3–1, 615–618.
38. Machado, J., A. Pinto, J. Santos, P. Monteiro, M. Violas, and L. Teixeira. 2004. Transversal filter model for high bit rate optical channel equalization. *Symposium on Enabling Optical Networks*.
39. Cariali, F., F. Martini, P. Chiappa, and R. Ballentin. 2000. Electronic compensation of PMD and chromatic dispersion with an IC 10 Gbit/s transmission system. *Electron. Lett.* 36:889–891.
40. Buchali, F., and H. Bulow. 2004. Adaptive PMD compensation by electrical and optical techniques. *J. Lightwave Tech.* 22:1116–1126.
41. Nakamura, M., H. Nosaka, M. Lda, K. Kurishima, and M. Tokumitsu. 2004. Electrical PMD equalizer ICs for 40-Gbit/s transmission. *Optical Fiber Communications (OFC) Conference*, Los Angeles, Paper TuG4.
42. Färbert, A. et al. 2004. Performance of a 10.7 Gb/s receiver with digital equaliser using maximum likelihood sequence estimation. *European Conference on Optical Communication*, Stockholm, Sweden.
43. Haunstein, H., A. Dittrich, and K. Sticht. 2004. Principles of electronic equalization of polarization-mode dispersion. *J. Lightwave Tech.* 22:1169–1182.
44. Machado, J., and A. Pinto. 2004. Algorithm for numerical eye opening evaluation. Submitted to *Conftele. Conference on Telecommunications (Conftele)*, Avaro, Portugal.
45. Bulow, H. 1999. Limitation of optical first-order PMD compensation. *Optical Fiber Communications (OFC) Conference*, San Diego, Technical Digest, 2:74–76.
46. Ozeki, T., M. Yoshimura, M. Teruhik, and H. Ibe. 1994. Polarization-mode-dispersion equalization experiment using a variable equalizing optical circuit controlled by a pulse-waveform-comparison algorithm. *Optical Fiber Communications (OFC) Conference*, San Jose, Paper TuN4.
47. Lee, S., R. Khosravani, J. Peng, V. Grubsky, D. Starodubov, A. Willner, and J. Feinberg. 1999. Adjustable compensation of polarization mode dispersion using a high-birefringence nonlinearly chirped fiber Bragg grating. *IEEE Photon. Techn. Lett.* 11:1277–1279.
48. Abe, I., H. Kalinowski, R. Nogueira, J. L. Pinto, and O. Frazao. 2003. Production and characterisation of Bragg gratings written in high-birefringence fibre optics. *IEE Proc. Circuits Devices Syst.* 150:495–500.

Biographies

Mário F. S. Ferreira was born in Ovar, Portugal. He graduated in physics from the University of Porto, Portugal, in 1984 and received his Ph.D. degree in physics from the University of Aveiro in 1992. At present, he is an associate professor at the physics

department of the University of Aveiro, where he leads a research group dedicated to the modeling and characterization of multi-section semiconductor lasers for coherent systems, quantum well lasers, optical fiber amplifiers and lasers, nonlinear effects and soliton propagation in optical fibers. He has written more than 150 scientific journal and conference publications, as well as a book with the title *Optics and Photonics* (in Portuguese). He is a member of the Optical Society of America (OSA), SPIE—The International Society for Optical Engineering, The New York Academy of Sciences (NYAS), the American Association for the Advancement of Science (AAAS), the European Optical Society (EOS), the European Physical Society (EPS), and the Portuguese Physical Society. He was a member of the editorial advisory committee of *Optics and Photonics News* (OSA) during 1999, being presently an associate editor of *Optical Fiber Technology—Materials, Devices, and Systems* (Elsevier), and a member of the advisory board of *Fiber and Integrated Optics* (Taylor & Francis) and *Nonlinear Optics* (Old City Publishing, Inc.).

Armando Nolasco Pinto was born in Oliveira do Bairro, Portugal, in 1971. He graduated in electronic and telecommunications engineering from the University of Aveiro, Portugal, in 1994, and received a Ph.D. degree in electrical engineering from the University of Aveiro in 1999. At present, he is an assistant professor at the electrical and telecommunications department of the University of Aveiro, and a researcher at the Institute of Telecommunications, Aveiro, Portugal. His main research interests focus on optical communication systems, mainly in nonlinear, polarization, and temperature-dependent effects in fiber optics. He has written more than 60 scientific journal and conference publications. He is a member of the Optical Society of America (OSA) of the Institute of Electrical and Electronics Engineers (IEEE).

Paulo Sérgio de Brito André was born in Luanda, Angola, in April 1971. He received a physics engineering degree in 1996 and the Ph.D. in physics in 2002, both from the Universidade de Aveiro, Portugal. In the same year he joined the Instituto de Telecomunicações—Aveiro as researcher. He is also an assistant professor at the University of Aveiro, teaching physics. His current research interests include the study and simulation of optoelectronics components, fiber Bragg gratings, transparent performance monitoring, multi-wavelength optical communications systems, and networks. Paulo André is a member of the Portuguese Physics Society (SPF) and of the Institute of Electrical and Electronics Engineers (IEEE).

Nelson J. Muga was born in Mogadouro, Portugal, in 1980. He received a physics degree from the University of Porto, Portugal, in 2002. He is currently pursuing an M.S. degree in applied physics at the University of Aveiro, Portugal. His current main interest of research is polarization effects in optical fibers.

José E. S. Machado was born in Leiria, Portugal, in 1978. He graduated in electrical and computer engineering from the University of Porto in 2002, Portugal, accomplishing his final graduation project in polymer optical fibers multiplexing techniques within COBRA Research Institute, Eindhoven University of Technology, Eindhoven, The Netherlands. After a short traineeship, in the core network department of VIP Snaga Komunikacije, Zagreb, Croatia, he joined PTInovação SA in 2003, carrying out most of his work at Instituto de Telecomunicações in Aveiro, Portugal. His main research interests are within electrical dynamic equalization in multi-gigabit optical networks.

Rogério Nunes Nogueira was born in Aveiro, Portugal, in 1976. He received a physics engineering degree in 1998 in the University of Aveiro. In the same year he joined the Instituto de Telecomunicações as a researcher in the field of optical communications. He is now finishing his Ph.D. research program in fiber Bragg gratings. His current research interests are fiber Bragg gratings, multi-wavelength optical devices, and

systems, optoelectronic devices and optical sensors. Rogério Nogueira is a member of the Portuguese Physics Society (SPF) and of the Institute of Electrical and Electronics Engineers (IEEE).

Sofia C. V. Latas was born in Évora, Portugal. She graduated in physics from the University of Lisbon in 1988 and became an assistant lecturer in the physics department of the University of Aveiro in 1989. At present, she is finishing her Ph.D. program at the University of Aveiro in the field of optical fiber solitons.

Mayra H. Sousa was born in Tuxpan, Veracruz, Mexico, in 1960. She graduated in physics and mathematics from the Polytechnic National Institute of Mexico City, Mexico, in 1981 and earned an M.Sc. degree from the same school in 1984. She is now completing her Ph.D. research program at the University of Aveiro in the field of dispersion-managed fiber solitons.

José R. F. da Rocha was born in Mozambique and received an M.Sc. degree in telecommunication systems and a Ph.D. in electrical engineering, both from the University of Essex, England, in 1980 and 1983, respectively. He is at present a full professor at the University of Aveiro, Portugal. He participates actively in the Telecommunications Institute, a national R&D non-profit organization, where he is a member of the management committee (Aveiro branch) and national coordinator for the optical communications area. He has coordinated the University of Aveiro and Telecommunications Institute participation in various projects included in the following European Union (EU) R&D Programs in the area of telecommunications: RACE, RACE II, ACTS, and IST. He has published approximately 170 papers, mainly in international journals and conferences and his present research interests include modulation formats and receiver design for very high capacity (above 40 Gbit/sec) optical communication systems based on linear and nonlinear transmission and WDM optical networks. In the past few years he has acted as a technical auditor, evaluator, and independent observer for the evaluation of projects submitted to various EU R&D programs. He has also participated in various project evaluation boards set up by the EPSRC (Engineering and Physical Sciences Research Council), United Kingdom. By invitation of the ACTS Management Committee, he participated in the Expert Groups on Visionary Research in Communications, aiming to create a bridge between the activities carried out in the 4th and the 5th Framework Programs on EU activities in the field of research, technological development, and demonstration.